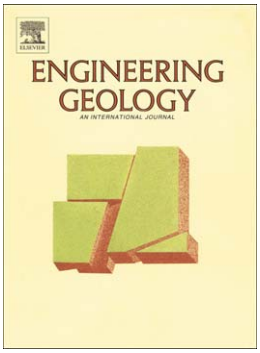

Source distribution of acoustic emissions during an in-situ direct shear test: Implications for an analog model of seismogenic faulting in an inhomogeneous rock mass

Tsuyoshi Ishida, Yuji Kanaori

PII: S0013-7952(09)00293-2
DOI: doi: 10.1016/j.enggeo.2009.11.003
Reference: ENGEO 3024

To appear in: *Engineering Geology*

Received date: 13 March 2009
Revised date: 28 August 2009
Accepted date: 14 November 2009

Please cite this article as: Ishida, Tsuyoshi, Kanaori, Yuji, Source distribution of acoustic emissions during an in-situ direct shear test: Implications for an analog model of seismogenic faulting in an inhomogeneous rock mass, *Engineering Geology* (2009), doi: 10.1016/j.enggeo.2009.11.003

Source distribution of acoustic emissions during an in-situ direct shear test: Implications for an analog model of seismogenic faulting in an inhomogeneous rock mass

Tsuyoshi ISHIDA, Kyoto University,

Tadashi KANAGAWA, Nittoc Construction Co., Ltd.,

and

Yuji KANAORI, Yamaguchi University

Keywords:
Rock; Fracture; Acoustic emission; Inhomogeneity; Asperity, Earthquake

ABSTRACT

We monitored acoustic emission (AE) events during an in-situ direct shear test on a specimen composed of a slate-dominant alternation of slate and sandstone, measuring 0.5 m long, 0.5 m wide and 0.2 m high. The test was conducted in a survey tunnel for an underground powerhouse in central Japan. The AE epicenters located on a fractured plane are compared with the locations of joints and a loosening seam, the height distribution of the fractured plane, and the horizontal movement of the test

block prior to failure. We conclude that an initially intact region of rock bounded by the joints and the seam is fractured, generating the AE. Considering these results in connection with asperity models of seismogenic faulting for a subduction-zone earthquake, the significant contrast of stress conditions derived from the geological inhomogeneity and the uneven fractured plane is analogous to that due to subducted seamounts and horst-graben structures on a subducted oceanic plate. For an inland earthquake, the intact regions on an expected shear plane can be considered to be a portion of the fault asperity that causes strong ground motion, while the weakened portion can be considered to correspond to a region of aseismic creep. Consequently, large-scale inhomogeneous rock fracturing experiments such as the in-situ direct shear test may provide useful insights as analog models of seismogenic faulting. Furthermore, understanding of inhomogeneous rock-mass fracturing obtained from such experiments will not only contribute to a better understanding of the mechanism of earthquakes but also provide valuable knowledge for AE monitoring applications in rock engineering, such as the predictions of rockbursts in mines and the monitoring of fractures around large underground chambers.

1. Introduction

Acoustic emission (AE) or microseismicity (MS) monitoring is a viable non-destructive method for detecting microfracturing prior to a macroscopic rock fracture. According to reviews by Hardy (1977) and Koerner et al. (1981), this monitoring method was used to evaluate the stability of rock masses in mines in the late 1930's (Hodgson, 1943; Obert and Duvall, 1946), and has been applied in investigations of rockbursts in mines (e.g., papers in Tang, ed. 2009). The method is currently being extended beyond mines to a wide variety of rock engineering problems including deep well fluid injection and extraction (Nicholson 1992), enhanced oil recovery (Jupe et al., 2000), hydraulic fracturing (Cornet, ed. 2007; Ishida et al., 2004), underground powerhouses (Ishida et al., 1995), tunnels (Hirata et al., 2007) and nuclear fuel waste disposal (Major and McEvilly, 1985). Among these applications, AE monitoring of slope stability has recently advanced for not only rock cliffs (Amitrano et al., 2005; Senfaute et al., 2003; Ishida et al., 2001) but also mudslides (Amitrano et al. 2007) by using active and passive waveguides, helping to overcome many of the difficulties associated with such monitoring (Dixon et al., 1996, 2003a, 2003b). However, AE occurrence itself strongly depends on geological conditions (Milev and Spottiswoode, 2002), as well as mining configurations (Senfaute et al., 1997, 2001). Thus, for successful AE monitoring, it is necessary to determine the key types of geological inhomogeneities and how they govern the locations of AE

events and the release of their seismic energy.

In seismology, asperity models (Lay and Kanamori, 1981; Lay et al., 1982) have been established, and many observations suggest the existence of an asperity or inhomogeneity of the fracturing process in not only subduction-zone earthquakes (Cloos, 1992; Estabrook et al., 1994; Cummins et al., 2002) but also inland earthquakes (Kamae and Irikura, 1998; Ma et al., 2001a; Utkucu et al., 2003). Accordingly, seismologists have accepted that geological inhomogeneity governs seismic energy release. On the other hand, laboratory experiments have attempted to clarify inhomogeneous fracture processes by comparing located AE sources with microscopic images (Lei et al., 2003) and X-ray tomographs (Young and Thompson, 2007). However, there are discrepancies between AE in laboratory experiments and real earthquakes. Therefore, experimental studies using large samples (Yoshida et al., 2004) and medium-scale field observations (e.g., Yamada et al., 2007) are very helpful to bridge such discrepancies.

As one such experiment, we monitored AE events during an in-situ direct shear test on a test block measuring 0.5 m long, 0.5 m wide and 0.2 m high having inherent natural geological inhomogeneities. The test was conducted in a survey tunnel for an underground powerhouse in central Japan and was part of a series of tests to determine the fracture criteria of the rock mass for the design of the underground chamber. The rock mass of the site consists mainly of an alternation of slate and sandstone, which belongs to the Mikura Formation of the Shimanto Supergroup of late

Cretaceous to Paleogene in age, and the test block was a slate-dominant alternation of slate and sandstone. Since the block included joints and a loosening seam, the fracturing process and AE clustering region were governed by these discontinuities. In addition, the test block rotated on the AE clustering region, which was a convex region (higher than the expected shear plane), as it approached the final fracture.

The test itself was conducted in March 1984, and thus the instruments used for the monitoring were outdated in comparison with current technology, although the date of the test is not important in relation to any other aspect of the present paper. At that time, the Tokyo Electric Power Company, which was responsible for power supply in this area, needed a new pumped storage hydroelectric power station as a power storage system to adjust for differences between supply and demand over time. The company completed the construction of the pumped storage hydroelectric power station in December 1999. From 1970 to 1990, with growth of the economy, many underground powerhouses were constructed in Japan. For planning purposes, many data of rock-mass properties were obtained through various tests including in situ measurements during excavations (e.g., Ishida et al., 1995; Ishida and Uchita, 2000). These data are invaluable for the investigation of inhomogeneous rock-mass fracturing. Among such data, the data from the in situ direct shear test described in the present paper are well preserved and arranged particularly well for analysis. These data also provide considerable geological information for discussion. Thus, we revisit the data and review relations between the located AE

events and geological inhomogeneity in connection with recent research results on rock fracturing processes and asperity models for earthquakes. We propose the possibility of an in-situ direct shear test as an analog model of seismogenic faulting in an inhomogeneous rock mass.

2. Geological setting

The test site was in a chamber that branches from a survey tunnel for an underground powerhouse constructed in Ohtsuki City, Yamanashi Prefecture, central Japan, as shown in Figure 1. The geology of the test site (see Figure 2) is mainly an alternation of slate and sandstone that belongs to the Mikura Formation of the Shimanto Supergroup (Kiho, 1987). The alternation strikes N60º to 70ºW and dips 60º to 70ºNE. The slate is dark gray to black in color and has well-developed schistosity. The sandstone is gray to light gray in color and is massive with less-developed bedding planes. Most of the fracture zones are parallel to the bedding plane. To the northeast, the rocks are underlain by sedimentary complexes of the Late Jurassic to Late Cretaceous. To the south, they are overlaid by an Eocene to Miocene sedimentary complex. To the west, there are intrusions of felsic plutonic rocks of the Pliocene.

As shown in Figure 3, the test site is located in a slate-dominant alternation of slate and sandstone (S*l*-DA), bounded on the northeast by a sandstone-dominant alternation of slate and sandstone (Ss-DA). Seven

faults can be identified in the area. They are referred to as F-A to F-F in this paper. The faults F-A, -F and -G have crushed zones a few meters thick. Six faults are nearly parallel to one another, having similar strikes (N50º to 77ºW) and dips (55º to 78º N). The direction almost corresponds to that of the bedding plane. The exception is fault F-D. In the direct shear test, the direction of the applied shear load was selected to be parallel to the strike of the bedding plane.

3. Specimen and testing method

3.1. Specimen

The specimen was a slate-dominant alternation of slate and sandstone (S*l*-DA) measuring 0.5 m long, 0.5 m wide and 0.2 m high, as shown in Figure 4. The specimen for the test block was made from the rock mass under the ground surface of the chamber by removing surrounding rocks outside the specimen using a small rotational boring machine and a mechanical breaker. No blasting was used, so as to avoid disturbing or loosening the specimen. The test block for the direct shear test was constructed by encapsulating the specimen in 0.1 m thick reinforced concrete. Three other test blocks were also constructed at neighboring positions in the chamber in the same way.

3.2. Testing method

Photo 1 shows a view of the direct shear test under preparation. A series of direct shear tests was conducted on the four specimens in order to obtain shear strength parameters (e.g. cohesion and internal friction angle) for planning the underground powerhouse.

Different magnitudes of vertical load, V=125, 250, 500 and 750 kN, were applied to the four specimens via a hydraulic ram connected to a hydraulic pump, and the vertical load was kept constant during the test. The magnitudes of the vertical load corresponded to 0.5, 1, 2, and 3 MPa as an averaged normal stress on the expected shear plane, which was the plane at the base of the specimen that extended from the ground surface around the specimen. In addition, a shear load, S, was applied in the direction parallel to the strike of the bedding plane. Since the direction of the shear load had an angle 17º from the horizontal, this load induced a normal stress component of S•sin17º/A on the expected shear plane as well as a shear stress component of S•cos17º/A along the plane, where A was the area of the expected shear plane. Thus, the normal stress on the expected shear plane was (V+S•sin17º)/A, and increased with the increasing of S in spite of V being held constant.

Over 5 minutes, S was increased by 80 kN and then held constant for the following 5 minutes. By repeating this 10-minute cycle, S increased until the specimen experienced a shear failure and started to slide along the expected shear plane. The testing method followed the guidelines for an

in-situ direct shear test published by JSCE (Japanese Society for Civil Engineers, Third Subcommittee in Committee on Rock Mechanics, 1978) and was almost the same as the suggested methods of the ISRM (International Society for Rock Mechanics, Commission on Standardization of Laboratory and Field Tests, 1981) with slight differences that included the block size and rate of shear displacement.

Figure 5 shows the results of a series of in-situ direct shear tests and the regression line. Assuming Coulomb's failure criterion, a regression line was obtained for the maximum shear stress, $S_o \cdot \cos 17^o / A$, and the maximum normal stress, $(V + S_o \cdot \sin 17^o)/A$, in each of the four tests, where S_o is the maximum shear load. From the obtained regression line, a cohesion of 3.16 MPa and an internal friction angle of 56.4º were obtained.

4. AE monitoring and displacement measurements

4.1. Outline and displacement gauges

The test block for which we monitored AE events was the block that was subjected to V = 500 kN. The positions of the AE sensors and displacement gauges are shown in Figure 4. Displacements were measured at ten points in total: four points (m, n, o and p) were for the shear displacement; another four points (i, j, k and l) were for vertical displacement; and the remaining two points (q and r) were for lateral displacement. Vertical and shear loads were measured by load cells set

between the rams and the test block. (see Photo 1).

4.2. AE sensors and their setting positions

A piezoelectric transducer consisting of PZT (Pb(lead) zirconium titanate) having a resonant frequency of 67 kHz was used as the sensor for AE monitoring. The PZT element was placed at the bottom of a cylindrical brass case with a diameter of 40 mm and height of 34 mm. The cylinder was filled with silicon rubber for waterproofing (Ishida et al., 1991). Since the dominant frequency of the waveform actually recorded in the test was in the range of 15 to 40 kHz, the resonant frequency of the sensor including the brass case should be within this frequency band.

As shown in Figure 4, eight AE sensors were fixed with cement paste in the bottom of the holes that were drilled around the test block; the holes had a diameter of 66 mm and depth up to 0.3 m

4.3. AE monitoring system

Photo 2 shows the AE-monitoring instruments. Since the test was conducted in 1984, the instruments were out of date compared to current state-of-the-art technology. Figure 6 is a schematic diagram of the AE monitoring system. An AE signal received at each AE sensor was amplified by 100 dB in total: 40 dB in a pre-amplifier and 60 dB in a main amplifier. The signal was then passed through a band-pass filter with a

frequency range from 5 to 100 kHz to eliminate noise and was recorded on a high-speed tape recorder. The tape recorder was used in direct recording mode with a tape speed of 76.2 cm/s, covering the frequency range set by the filter.

The recorded AE signals were replayed at a tape speed of 1.19 cm/s, which was 1/64 of the recording tape speed. The replayed AE signals were converted to digital data with an amplitude resolution of 10 bit and a sampling time of 50 μs, which was equivalent to 0.78 μs in real time. The AE event rates were determined from the wave signals reproduced from the recorded tape by setting a constant discrimination level of 0.6 volts.

5. Characteristics of the fracture surface plane

After the test, the upper part of the test block that separated along the fractured plane was removed. Then, the height distribution of the lower fracture plane was measured and geological inhomogeneity was surveyed. Figure 7 shows the height distribution of the fracture plane. Figure 7a shows a contour map that reveals the deviation from the expected shear plane corresponding to the ground surface around the specimen. The heights were measured at grid points by covering the fracture plane with a 1 m^2 wooden frame having a 2-cm interval wire grid. The hatched parts in Figure 7a show the concave regions that were lower than the ground surface, and the open part shows the convex region that was higher than the ground surface. To verify the measured heights, the upper part of the test

block was turned over and the heights of the opposite side fractured plane were also measured. Figure 7b shows three sectional views of the fracture plane.

Figure 8 shows a sketch of the joints and the loosing seam on the lower fracture surface plane. The intact part bounded by the two joints J-2 and J-3, having dips of 21ºW and 52ºW, and by the loosening seam Sm-1, appears to correspond to the raised part around the convex region (height ≥ +3 cm) in the upper right of Figure 7.

Photo 3 shows the fractured plane of the upper part of the test block that was removed and turned over. This photo was printed by turning over the negative so that the left and right hand sides (with respect to the direction of the shear load) of the photo correspond with those of Figures 7 and 8. The features of the upper fracture plane shown in Photo 3 correspond to the joints and loosening seam observed on the lower fracture plane shown in Figure 8.

6. Results

6.1. AE event rates, load and displacements

The test lasted 6 hours and 40 minutes. Figure 9 shows the shear load, the shear and vertical displacements, and the AE event rates at intervals of 20 minutes. The AE event rates are averages of those counted

at sensors 4 and 2 (see Figure 4), which were selected as good examples of sensors located in the vicinity of the shear loading plate and on the opposite side from it, respectively. AE events were not recorded for some periods, shown by the black bars in the upper part of Figure 9, due to replacing a recording tape and other reasons. The AE event rates in the period are estimated from those immediately before and after the periods with no recorded data, and are shown using broken lines.

Between 200 and 220 minutes, the AE event rate suddenly increased and then returned to the lower level again. It gradually increased again from around 280 or 300 minutes, and a burst of AE events occurred after 380 min, leading up to the final failure of the test block.

The period around 280 or 300 minutes roughly corresponds to the time when the vertical average displacements at points i and j (see their positions in Figure 4) in the vicinity of the shear loading plate changed from downward to upward. The period after 380 minutes corresponds to the time when the vertical average displacements at points k and l at the opposite side to the shear loading plate changed from downward to upward. Thus, the AE activity corresponded to the change in the vertical displacement from downward to upward, which indicates the onset of the final failure of the test block, as has been observed in many in-situ direct shear tests (Hirama et al., 1983).

As described in the following section, AE events whose sources were located with a sufficient level of accuracy were recorded only in the 22 minutes prior to failure. Figure 10 shows AE event rates every 10 seconds

and the change of the shear load during these 22 minutes. The AE event rates are the average of those counted at sensors 2 and 4, as shown in Figure 9. Between Figures 10a and 10b, there is a gap of 3 minutes 33 seconds, corresponding to a lack of AE measurement due to replacement of the recording tape. The bars on the lateral bottom axes in the figures indicate the occurrence times of AE events for which sources were located.

6.2. Two-dimensional source location of AE events

Due to the limitation of the test configuration, we could not place an AE sensor just above or below the expected shear plane. All sensors were located lower than the expected shear plane around the test block. When performing simulations of the three-dimensional source locations for the sensor distribution, it was found that small errors in reading P-wave arrival times resulted in serious errors in determining source locations in the vertical direction. However, the reading errors resulted in only small errors in determining source locations in the horizontal direction (Ishida, 1999). Fortunately, all AE events that occurred in this test are thought to have been generated in a thin layer, only in a few centimeters thick, parallel to the expected shear plane, since the heights of fractured plane range lie within -3 to +5cm of the expected shear plane as shown in Figure 7. Consequently, AE sources were located two-dimensionally under the assumption that they were generated on the expected shear plane. In this case, since the P-wave velocity of the rock around the test block was

measured to be 5.0 km/s by using PZT transmitters set at both lateral sides of the test block, the unknown parameters for the source location are the two-dimensional (2D) source coordinates, x and y, and the occurrence time of the AE event, t. If the arrival time of P-wave initial motion was detected from waveforms at more than four sensors, these three unknown parameters can be determined by a non-linear least squares method.

AE sources were located with an accuracy expected to fall within 50 mm. This was possible because we used only AE events satisfying the condition that standard deviation of differences between the observed and back-calculated arrival times were within 10 micro-seconds. Most AE events whose P-wave initial motions were detected at more than four sensors and that satisfied the condition of the standard deviation were recorded just prior to the final failure. Consequently, the AE sources were located only for the period of 22 minutes before the final failure, which was indicated by the sudden decrease of the shear load.

Figure 11 shows examples of recorded waveforms. The AE event occurred at around 70 s prior to the failure. The arrow on each waveform indicates an arrival time that was interpreted as P-wave initial motion.

A total of 403 AE events were examined and the epicenters of 154 AE events were located as shown in Figure 12. An AE clustering region appears in the upper right of the figure, corresponding to the intact part in Figure 8 bounded by the two joints J-2 and J-3 and the loosening seam Sm-1. It also corresponds to the raised part around the convex region with height $\geq +3$ cm in the upper right of Figure 7. This suggests that AE

clustering occurred in an intact region.

6.3. Horizontal locations of the test block prior to failure

Figure 13 shows the horizontal location of the test block every 20 minutes prior to failure and at 1 minute after failure, to examine the block movement. The displacement of the block is enlarged in comparison with the block size, as shown in the scale of the figure. The δx and δy displacements are averages calculated by

$$\delta x = \frac{Ur + Uq}{2} \quad \text{and} \quad \delta y = \frac{Um + Un + Uo + Up}{4},$$

where *Ur, Uq, Um, Un, Uo* and *Up* are displacements measured in mm at the gauges r, q, m, n, o and p, as shown in Figure 4. The block rotation angle, θ, is also shown with an exaggeration of approximately 17.4 times larger than the real angle given by

$$\theta = 1.0 \times 10^3 \times Arc\tan\left(\frac{Un - Up}{500}\right) = 17.4 \times \frac{360}{2\pi} \times Arc\tan\left(\frac{Un - Up}{500}\right), \quad (\theta : \text{degree}).$$

This figure indicates that the large displacement and rotation were induced after 23 minutes prior to the failure, which roughly corresponds to the period after 22 minutes when the epicenters of the AE events shown in Figure 12 were recorded. When we compare the rotation of the test block shown in Figure 13 to the contour map of the fractured plane as shown in Figure 7, the test block seems to rotate around the convex region of +3 cm height in the upper right of the figure.

7. Discussion

7.1. Test block fracturing governed by inhomogeneity

AE events were monitored during an in-situ direct shear test for a specimen consisting of a slate-dominant alternation of slate and sandstone measuring 0.5 m long, 0.5 m wide and 0.2 m high. The 2D locations were determined under the assumption that they were generated on the expected shear plane, the level of which was equal to the ground surface around the specimen. The AE clustered in the upper right of the test block corresponded to an intact region bounded by two joints and a loosening seam, as shown in Figure 8. The region where the AE sources cluster also corresponded to the raised part around the convex region of height ≥ +3 cm in the upper right of the test block, and the test block rotated around this convexity, as shown in Figure 13. These results demonstrate that the fracturing process of the test block and the AE clustering region were strongly governed by the inherent inhomogeneity of the test block.

7.2. Similarity to a subduction-zone earthquake

The fact that the fracturing processes of earthquakes depend strongly on geological inhomogeneities has become well known recently. For example, Cloos (1992) proposed a model of a subduction-zone earthquake in which seamounts jammed against the base of the overriding plate act as

strong asperities that rupture by stick-slip faulting. He suggested that asperities which characterize high moment release have areas of less than 10% of the total rupture areas. Such asperities are thought to be long-lived features and are confirmed to be fixed in space throughout seismic cycles (e.g., Yamanaka and Kikuchi, 2004). The persistent geometric irregularities and material contrast produce significant contrast of stress condition due to subducted seamounts (Cloos, 1992) and horst-graben structures (Ruff, 1989) on the subducted oceanic plate. Estabrook et al. (1994) also pointed out that subduction of seamounts in the Gulf of Alaska seamount province may explain the location, moment, focal mechanism, and depth of five earthquakes with moment magnitudes 6.93 to 7.03. Cummins et al. (2002) suggested that subducted seamounts might have acted as a strong barrier during the 1946 Nankai earthquake but may rupture as an asperity in a future earthquake.

The aspect ratio (height/width) of the contact surface between the ground surface and the specimen was ~0.1 (see Figure 7), whereas the ratio of seamount height to diameter was ~0.05 (see Figure 3A in Cloos, 1992) and 0.14 on average from global ship-track bathymetry data (Hiller and Watts, 2007). A similar aspect ratio of ~0.07 (a 4 km high and 60 km wide seamount) was used for a seamount subduction model by Scholz and Small (1997). Cloos (1992) also pointed out that the seamount surface slopes commonly range from 5° for tall ones to > 10° for short ones, which is roughly comparable with the surfaces shown in Figure 7(b). Although large subduction earthquakes are not always associated with subducted

seamounts, our tests that are analogous to these subduction earthquakes are expected to provide insights for earthquake forecasting with respect to spatial and temporal evolution of seismicity prior to a large earthquake. Furthermore, relatively smoothed subducted seafloor seems to have even caused the stress inhomogeneity in the plate interface due to the variety of contact conditions and small scale asperities. Recent discoveries of small-to-moderate repeating earthquakes along the subduction zone in Japan (Uchida et al., 2003) and in the longitudinal valley fault in Taiwan (Chen et al., 2009) suggest that there are small to moderate size asperities highly stressed by surrounding creeping zones on a fault plane, as reported for the Parkfield sections of the San Andreas fault (Nadeau and McEvilly, 1999). This suggests that shear stressing rates inside, at the margins of, and outside small asperities are extremely different and thus produce significant inhomogeneous stress conditions similar to our tests.

One point to consider is that friction and creep are at a higher temperature in subduction zones, whereas friction and brittle asperities breaking were at room temperature in the test reported here. However, the brittle behavior of the earth's crust is kept until the depth of about 600°C unlike 300°C for quartz-rich continental plate, since the oceanic lithosphere consists of mafic rocks and is expected to have an olivine-rich rheology. The thickness of the seismogenic brittle layer is also proportional to the age of the oceanic plate, which then cools the overlying continental crust and deepens the seismogenic depth along the plate interface. Therefore, brittle failures normally occur in subduction zones as deep as several tens of

kilometers, while another mechanism has been proposed for earthquakes that occur for the slabs deeper than ~100 km, as explained in detail by Scholz (1990).

Fluid plays a role as a lubricant agent along the plate interface, and subducted sea floor covered by water-rich sediments, in particular, is expected to reduce fault friction, which cannot be reproduced in this test. However, as mentioned above, the highly irregular contact geometry of the specimen instead plays a major role in causing the significant inhomogeneity of shear stress. Scholz and Small (1997) speculate that subduction of a large seamount increases the normal stress across the interface and thus enhances seismic coupling. Thus, we believe that the fluid effect would be minor, but large-scale inhomogeneities such as those in our test are the primary factor controlling earthquake rupture.

7.3. Similarity to an inland earthquake

As well as the analogy to a subduction earthquake, we also propose that the experimental slip of our specimen is similar to the occurrence of an inland earthquake. Even though seamount-like strong heterogeneity is uncommon in an inland environment, there are many studies that have found significant asperities on an earthquake source fault. Kamae and Irikura (1998) simulated the strong ground motion of the January 17, 1995 Mw=6.9 Hyogo-ken Nanbu (Kobe) earthquake with a source model consisting of three asperities on the fault plane. Ma et al. (2001a) successfully simulated

near-source strong-motion records, broadband teleseismic displacement waveforms, and well-distributed Global Positioning System (GPS) data of the September 20, 1999 Mw=7.6 Chi-Chi (Taiwan) earthquake using their two-segment asperity model. Moreover, Utkucu et al. (2003) inverted the teleseismic P and SH waveforms of the June 6, 2000 Ms=6.1 Orta earthquake in central Anatolia, Turkey, using their two segment asperity model. Somerville et al. (1999) compiled source models of the recent inland crustal earthquakes and concluded that asperity area is only about 20% of the entire rupture plane, which is more or less similar to the relation suggested by Cloos (1992) for subduction zone earthquakes. As shown in this paper, the test block of an in-situ direct shear test usually has both intact and weakened regions on an expected shear plane due to its inherent inhomogeneity. If the intact region is considered to correspond to a portion of asperity that causes strong ground motion and the weakened region is considered to correspond to a region of aseismic creep, an in-situ direct shear test could be a good analog model for an inland earthquake fault.

7.4. Possibility of an analog model of seismogenic faulting

To compare our experiment with earthquake occurrence, one may ask whether the magnitude of the normal stress, 0.5-3 MPa, for the tests is comparable with not only an inland earthquake but also a subduction-zone earthquake. However, it could be thought that the magnitude of the stress for the tests is comparable with differential (deviatoric) stress at the

seismogenic depth in both subduction and shallow intraplate environments. Allmann and Shearer (2009) investigated the global variation of earthquake stress drops and showed that the stress drop estimates for individual earthquakes range from 0.3 to 50 MPa and the median is about 4 MPa independent from magnitude. Intriguingly, they found that the stress drop for the subduction zone earthquakes is a factor of 2 smaller than those for inland earthquakes. The earthquake stress drop could possibly be a fraction of the regional differential stress. However, there are many reports that clearly show stress tensor rotations due to mainshock faulting near the source fault. For example, Hardebeck and Hauksson (2001) analyzed aftershock focal mechanisms of the 1992 Mw=7.4 Landers, California earthquake and demonstrated remarkable rotation of principal stress axes near the mainshock source faults. Such evident stress disturbance implies that the mainshock's stress drop should be comparable with the regional differential stress to have significant stress perturbation associated with coseismic deformation (King et al., 1994). If the stress drop were significantly small relative to the regional deviatoric stress, stress perturbation and stress tensor rotations would not have occurred along the rupture zone.

It is interesting to note that the movement of the test block in Figure 13 exhibited a phase in which the precursory slip accelerated to the final failure, which is similar to the nucleation process in the rate- and state-dependent friction law derived from laboratory experiments with smoothed contact of rock samples (Dieterich, 1972, 1994). With the

above discussion on analogy to the stress magnitude of the earthquakes, it seems to be really important to note that the kinematics with highly irregular fault surface follows the rate- and state- friction pervasive in seismology. It would shed a light on the possibility to detect the precursory deformation for not only a subduction-zone earthquake but also an inland earthquake.

Foreshock activity prior to a main shock has often been reported and might be associated with the slip acceleration phase in the earthquake nucleation process (Dieterich, 1994). Recent studies on earthquake triggering and large earthquake doublets (e.g., Stein, 1999), as well as the proposed seismicity patterns in a rupture cycle (Scholz, 1988), suggest that a large earthquake is normally initiated from a high seismicity area, which is influenced by previous shocks or possibly precursory activity due to a nucleation slip, and then propagates to the strongly locked areas (asperities) where lower seismicity is observed. Considering such scenarios that have been observed in many earthquakes, the observed AE sources in our test are indeed analogous to foreshock activity and appear to be located on the margin of the loosening seam that corresponds to a creeping zone of a seismogenic fault planes (see Figure 12, cf. Figure 8). In particular on an inland earthquake, the observed AE sources of the test appear to be on the margin of the lower (concave) part of the fractured plane that might cause a large slip at the final failure corresponding to the mainshock of an earthquake (see Figure 12, cf. Figure 7). This analogy would be useful for predicting a mainshock from foreshock activity.

We believe that large-scale inhomogeneous rock fracturing experiments like the present in-situ direct shear test have the possibility to provide useful insights from new aspects as analog models of seismogenic faulting, in addition to the models proposed by Mogi (2007), Scholz (1990) and others based on tests of small homogeneous core samples. Moreover, recent advances in monitoring methods (Young and Thompson, 2007; Nishizawa et al., 1997) and in simulation and analysis methods for seismograms (Estabrook et al., 1994; Kamae and Irikura, 1998; Ma et al., 2001a; Utkucu et al., 2003) and AE waveforms (Linzer, 2005; Ma et al., 2001b) enhance the utility of large-scale inhomogeneous rock fracturing experiments. Understanding rock fracturing through such efforts would also provide invaluable information for successful AE monitoring applications in rock engineering, such as the prediction of rockbursts in mines and the monitoring of fractures around large underground chambers.

8. Concluding remarks

We monitored AE events during an in-situ direct shear test conducted in a survey tunnel for an underground powerhouse. AE epicenters located on the fractured plane were compared with the location of joints and a loosening seam, the distribution of heights of the fractured plane, and the horizontal movement of the test block. Furthermore, we discussed the results in connection with asperity models for seismogenic faulting. The

following results were obtained.

(1) The AE count rate increase corresponded to the change in the vertical displacement from downward to upward, which indicated the onset of the final failure of a test block, as has been observed in many in-situ direct shear tests.

(2) The AE clustering region corresponded to the region of intact rock surrounded by the joints and the loosening seam. The AE clustering region also corresponded to a convex region (higher than the expected shear plane). The measurement of horizontal displacement indicated that the test block rotated around this convex region in the final fracturing stage.

(3) These experimental results were discussed in relation to recently advanced asperity models for an earthquake. For a subduction-zone earthquake, the significant contrast of stress condition derived from geological inhomogeneity and the uneven fractured plane is analogous to that due to subducted seamounts and horst-graben structures on the subducted oceanic plate. Thus, the analogy is expected to provide insights into earthquake forecasting with respect to the spatial and temporal evolution of seismicity prior to a large earthquake.

(4) For an inland earthquake, the intact regions of an expected shear plane could be considered to be a portion of the fault asperity that causes strong ground motion, while the weakened portion could be considered to correspond to a region of aseismic creep. Thus, the in-situ direct shear test is possibly a good analog model for an inland earthquake fault.

(5) The acceleration phase of the precursory slip to the final failure

observed in the movement of the test block was similar to the nucleation process in regard to the rate- and state-dependent friction law derived from laboratory experiments with smoothed contact of rock samples. The foreshock activity prior to a main shock that has often been reported might be associated with a slip acceleration phase in the earthquake nucleation process. Thus, the analogy between the AE sources observed in our test and the foreshock activity could allow the prediction of mainshocks from foreshock activity.

(6) Large-scale inhomogeneous rock fracturing experiments such as the in-situ direct shear test have the possibility to provide useful insights as analog models of seismogenic faulting. Furthermore, understanding inhomogeneous rock-mass fracturing obtained through such efforts would provide not only better understanding of the mechanism of earthquakes but also invaluable knowledge for AE monitoring applications in rock engineering, such as the prediction of rockbursts in mines and the monitoring of fractures around large underground chambers.

Acknowledgements

When we conducted the in-situ direct shear test, we obtained technical support from many employees of The Tokyo Electric Power Company, Incorporated, Nippon Koei Co., Ltd. and Central Research Institute of Electric Power Industry. We would like to thank them for their help and suggestions. We also acknowledge Dr. Shinji Toda of the Disaster Prevention Research Institute, Kyoto University, for his invaluable comments on the comparison between the test and seismogenic faulting.

REFERENCES

Allmann, B. P., and Shearer, P. M., 2009, Global variations of stress drop for moderate to large earthquakes, Journal of Geophysical Research 114, B01310, doi:10.1029/2008JB005821.

Amitrano, D., Gaffet, S., Malet, J.-P. and Maquaire, O., 2007. Understanding mudslides through micro-seismic monitoring: The Super-Sauze (South French Alps) case study. Bulletin de la Société Géologique de France 178(2), 149-157.

Amitrano, D., Grasso, J.R. and Senfaute, G., 2005. Seismic precursory patterns before a cliff collapse and critical-point phenomena. Geophysical Research Letters 32(8), L08314, doi:10.1029/2004GL022270.

Chen, K. H., Rau, R. -J. and Hu, J. –C., 2009, Variability of repeating earthquake behavior along the Longitudinal Valley fault zone of eastern Taiwan, Journal of Geophysical Research 114, B05306, doi:10.1029/2007JB005518.

Cloos, M., 1992. Thrust-type subduction-zone earthquakes and seamount asperities: A physical model for seismic rupture, Geology 20, 601-604.

Cornet, F.H. (ed.), 2007, Special Issue: Induced Seismicity, International Journal of Rock Mechanics and Mining Sciences 44, 1077-1171.

Cummins, P. R., Baba, T., Kodaira, S. and Kaneda, Y., 2002. The 1946

Nankai earthquake and segmentation of the Nankai Trough, Physics of the Earth and Planetary Interiors 132, 75-87.

Dieterich, J., 1972, Time dependent friction in rocks, Journal of Geophysical Research 77, 3690-3697.

Dieterich, J., 1994, A constitutive law for rate of earthquake production and its application to earthquake clustering, Journal of Geophysical Research 99, 2601-2618.

Dixon, N., Hill, R. and Kavanagh, J., 2003a. Acoustic emission monitoring of slope instability: development of an active waveguide system. Geotechnical Engineering 156(2), 83-95.

Dixon, N., Kavanagh, J. and Hill, R., 1996. Monitoring landslide activity and hazard by acoustic emission. Journal of the Geological Society of China 39(4), 437-464.

Dixon, N., Spriggs, M., Hill, R. and Kousteni, A., 2003b. Acoustic emission techniques for locating shear surfaces forming with slopes, Proc. of 1st. International Conference on Fast Slope Movement Prediction and Prevention for Risk Mitigation, Naples, Italy, 163-168.

Estabrook, C. H., Jacob, K. H. and Sykes, L. R., 1994. Body wave and surface wave analysis of large and great earthquakes along the Eastern Aleutian Arc, 1923-1993: Implications for future events, Journal of Geophysical Research 99, B6, 11643-11662.

Geological Survey of Japan, AIST (ed.), 2007. Seamless Digital Geological Map of Japan 1: 200,000. May 12, 2007 version. Research Information Database DB084, Geological Survey of Japan, National Institute of Advanced Industrial Science and Technology.

Hardebeck, J. L. and Hauksson, E., 2001, Crustal stress field in southern California and its implications for fault mechanics, Journal of Geophysical Research 106, 21859-21882.

Hardy, H.R., 1977. Emergence of acoustic emission / microseismic activity as a tool in geomechanics. Proceeding of the First Conference on Acoustic Emission/Microseismic Activity in Geologic Structures and Materials, University Park, Pennsylvania, USA, 13-31.

Hillier, J. K. and Watts, A. B., 2007, Global distribution of seamounts from ship-track bathymetry data, Geophysical Research Letters 34, L13304, doi:101029/2007GL029874.

Hirama, K., Maruyama, M. and Kuwabara, T., 1983. Application of acoustic emission to rock testing, Report of the Technical Research Institute Ohbayashi Corporation 27, 102-106. (in Japanese)

Hirata, A., Kameoka, Y. and Hirano, T., 2007. Safety management based on detection of possible rock bursts by AE monitoring during tunnel excavation, Rock Mechanics and Rock Engineering 40, 563-576.

Hodgson, E. A., 1943. Recent developments in rockburst research at Lake Shore Mines, Transactions of the Canadian Institute of Mining and Metallurgy 46, 313-324.

International Society for Rock Mechanics, Commission on Standardization of Laboratory and Field Tests, 1981. Suggested methods for determining shear strength in rock characterization testing and monitoring (ISRM suggested methods), Brown, E. T. (ed.), 129-140. Pergamon Press, Oxford, England.

Ishida, T., 1999. An introduction of acoustic emission of rock, Kinmiraisha, p.213 (in Japanese)

Ishida, T., Chen, Q., Mizuta, Y. and Roegiers, J-C., 2004. Influence of fluid viscosity on the hydraulic fracturing mechanism. Transactions of the ASME, Journal of Energy Resource Technology 126, 190-200.

Ishida,T., Kanagawa,T., Tsuchiyama,S. and Momose,Y., 1991. High frequency AE monitoring with excavation of a large chamber. Proceedings of the Fifth Conference on Acoustic Emission/Microseismic Activity in Geologic Structures and Materials, University Park, Pennsylvania, USA, 479-490.

Ishida, T., Kanagawa T., Uchita Y. and Urayama M., 1995. Acoustic emission mechanism and rock-mass behavior as deduced from in situ measurements during progressive excavation of an underground powerhouse, Proceedings of the Eighth International Congress on Rock Mechanics, Tokyo, 593-596.

Ishida, T., Nishikawa, T., Tanaka, M. and Shiotani, T., 2001. Acoustic emission monitoring for an unstable rock mass left after slope failure, Proceedings of Fifth International Symposium on Rockburst and Seismicity in Mines, Magaliesberg, South Africa, 29-33.

Ishida, T. and Uchita, Y., 2000. Strain monitoring of borehole diameter changes in heterogeneous jointed wall rock with chamber excavation; estimation of stress redistribution, Engineering Geology 56, 63-74.

Japan Society of Civil Engineers, Third Subcommittee in Committee on Rock Mechanics, 1978. Guide line for in-situ direct shear test, Proc. of the Japan Society of Civil Engineers 11, 37-46. (in Japanese)

Jupe, A., Jone, R., Wilson, S. and Cowles, J., 2000. The role of microearthquake monitoring in hydrocarbon reservoir management, SPE63131, Proc. of 2000 Society of Petroleum Engineers Annual Technical Conference and Exhibition, Dallas, Texas.

Kamae, K. and Irikura, K., 1998. Source model of the 1995 Hyogo-ken Nanbu earthquake and simulation of near-source ground motion, Bulletin of the Seismological Society of America 88, 2, 400-412.

Kiho, K., 1987. Geological survey report of Kazunogawa pumped storage power station site (No.2), CRIEPI(Central Research Institute of Electric Power Industry) Report U86512, p.31 (in Japanese)

King, G. C. P., Stein, R. S. and Lin, J., 1994, Static stress changes and the triggering of earthquakes, Bulletin of the Seismological Society of America 84, 935-953.

Koerner, R. M., McCabe, W. M. and Lord, A. E. Jr., 1981. Overview of acoustic emission monitoring of rock structures. Rock Mechanics 14, 27-35.

Lay, T., and Kanamori, H., 1981. An asperity model of large earthquake sequences, In Earthquake Prediction and International Review, Simpson, D. and Richard, P. (ed.), Maurice Ewing Series, 4, AGU, Washington, D. C., 579-592.

Lay, T., Kanamori, H. and Ruff, L., 1982. The asperity model and the nature of large subduction zone earthquakes, Earthquake Pred. Res. 1, 3-71.

Lei, X., Kusunose, K., Satoh, T. and Nishizawa, O., 2003. The hierarchical rupture process of a fault: an experimental study, Physics of the Earth and Planetary Interiors 137, 213-228.

Linzer, L. M., 2005. A relative moment tensor inversion technique applied to seismicity induced by mining, Rock Mechanics and Rock Engineering 38, 81-104.

Ma, K-F., Mori, J. Lee, S-J. and Yu, S. B., 2001a. Spatial and temporal distribution of slip for the 1999 Chi-Chi, Taiwan, earthquake, Bulletin of the Seismological Society of America 91, 5, 1069-1087.

Ma, X. O., Cho, S. and Takemoto, M., 2001b. Acoustic emission source analysis of plasma sprayed thermal barrier coatings during four-point bend tests, Surface and Coating Technology 139, 55-62.

Major, E. L. and McEvilly, T. V., 1985. Acoustic emission and wave propagation monitoring at the spent fuel test: Climax, Nevada, International Journal of Rock Mechanics and Mining Science & Geomechanical Abstracts 22, 215-226.

Milev, A. M. and Spottiswoode, S. M., 2002. Effect of the rock properties on mining-induced seismicity around the Ventersdorp Contact Reef, Witwatersrand basin, south Africa, Pure and Applied Geophysics 159, 165-177.

Mogi, K., 2007, Experimental rock mechanics, Taylor & Francis, p.361

Nadeau, R. M. and McEvilly, T. V., 1999, Fault slip rates at depth from recurrence intervals of repeating microearthquakes, Science 285, 718-721, doi:10.1126/science.285.5428.718.

Nicholson, C., 1992. Earthquakes associated with deep well activities --Comments and case histories--, Proc. of the 33rd US Rock Symposium, Santa Fe, USA, 1079-1086.

Nishizawa, O., Satoh, T., Lei, X. and Kuwahara, Y., 1997. Laboratory studies of seismic wave propagation in inhomogeneous media using a laser Doppler vibrometer, Bulletin of the Seismological Society of America 87, 4, 809-823.

Obert, L. and Duvall, W. I., 1946. Microseismic method of predicting rock failure in underground mining, parts I and II, R. I. 3797 and 3803, USDI, Bureau of Mines.

Tang, C. (ed.), 2009. Proceedings of the Seventh International Symposium on Rockburst and Seismicity in Mines, p.1611, Dalian, China.

Ruff, L. J., 1989, Do trench sediments affect great earthquakes occurrence in subduction zones?, Pure and Applied Geophysics 129, 1/2, 263-282.

Scholz, C. H., 1988, Mechanisms of seismic quiescences, Pure and Applied Geophysics 126, 701-718.

Scholz, C. H., 1990, The mechanics of earthquakes and faulting, Cambridge Univeristy Press, p.439

Scholz, C. H., and Small C., 1997, The effect of seamounts subduction on seismic coupling, Geology, 25, 487-490.

Senfaute, G., Al-Heib, M., Josien, J.P. and Noirel, J.F., 2001. Detection and monitoring of high stress concentration zones induced by coal mining using numerical and microseismic methods, Proc. of 5th Symposium on Rockburst and Seismicity in Mines, Johannesburg, South Africa, 453-456.

Senfaute, G., Chambon, C., Bigarre, P., Guise, Y. and Josien, J.P., 1997. Spatial Distribution of Mining Tremors and the Relationship to Rockburst Hazard. Pure and Applied Geophysics 150, 451-459.

Senfaute, G., Merrien-Soukatchoff, V., Morel, J. and Gourry, J.C., 2003. Microseismic monitoring applied to prediction of chalk cliffs and contribution of numerical modelling, Proc. of 1st. International Conference on Fast Slope Movement Prediction and Prevention for Risk Mitigation. Bologna, Naples, Italy, 463-468.

Somerville, P. G., Irikura, K. Graves, R., Sawada, S., Wald, D., Abrahamson, N., Iwasaki, Y., Kagawa, T., Smith, N. and Kowada, A.,

1999, Characterizing crustal earthquake slip models for the prediction of strong ground motion, Seismological Research Letters 70, 59-80.

Stein, R. S., 1999, The role of stress transfer in earthquake occurrence, Nature 402, 605-609.

Utkucu, M., Alptekin, Ö. and Pinar, A., 2003. A detailed source study of the the Orta(Çankiri) earthquake of June 6, 2000 (Ms=6.1): An intraplate earthquake in central Anatolia, Journal of Seismology 7, 193-202.

Uchida, N., Matsuzawa, T. and Hasegawa, A., 2003, Interplate quasi-static slip off Sanriku, NE Japan, estimated from repeating earthquakes, Geophysical Research Letters 30(15), 1801, doi:10.1029/2003GL017452.

Yamada, T., Mori, J.J., Ide, S., Abercrombie, R. E. Kawakata, H., Nakatani, M. Iio, Y. and Ogasawara, H., 2007. Stress drops and radiated seismic energies of microearthquakes in a South Africa mine, Journal of Geophysical Research 112, B03305, doi:10.1029/2006JB004553.

Yamanaka, Y. and Kikuchi, M., 2004, Asperity map along the subduction zone in northeastern Japan inferred from regional seismic data, Journal of Geophysical Research 109, B073007, doi:10.1029/2003JB002683.

Yoshida, S., Kato, A., Kato, N. and Nakatani, M., 2004. Interpretation of various slip modes on a plane boundary based on laboratory and numerical experiments, Earth Planets Space 56, 795-801.

Young, R. P. and Thompson, B. D., 2007. Imaging dynamic fracture with acoustic emission and x-ray tomography. Proceedings of the Eleventh Congress for International Society for Rock Mechanics, p.1481, Specialized Session 04--Application of Geophysics to Rock Engineering (CD Rom), Lisbon, Portugal.

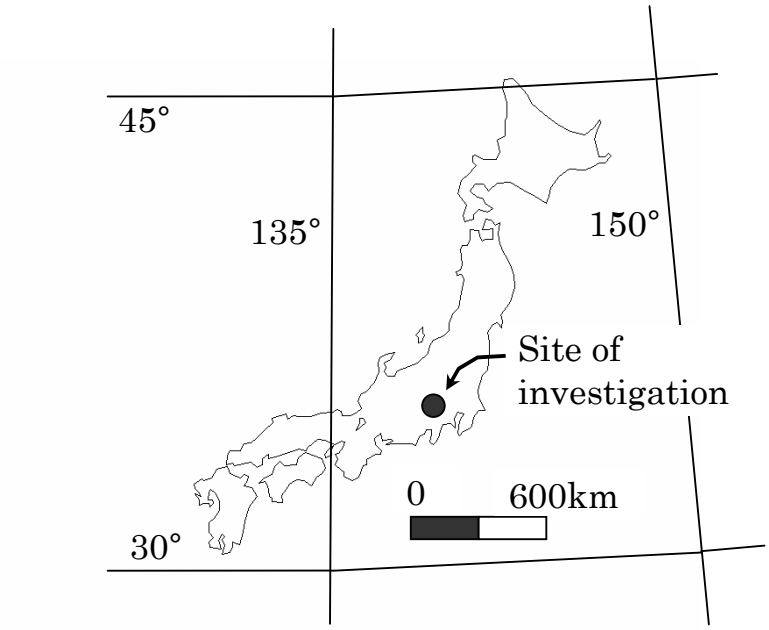

Figure 1 Map of Japanese islands and location of the site of investigation.

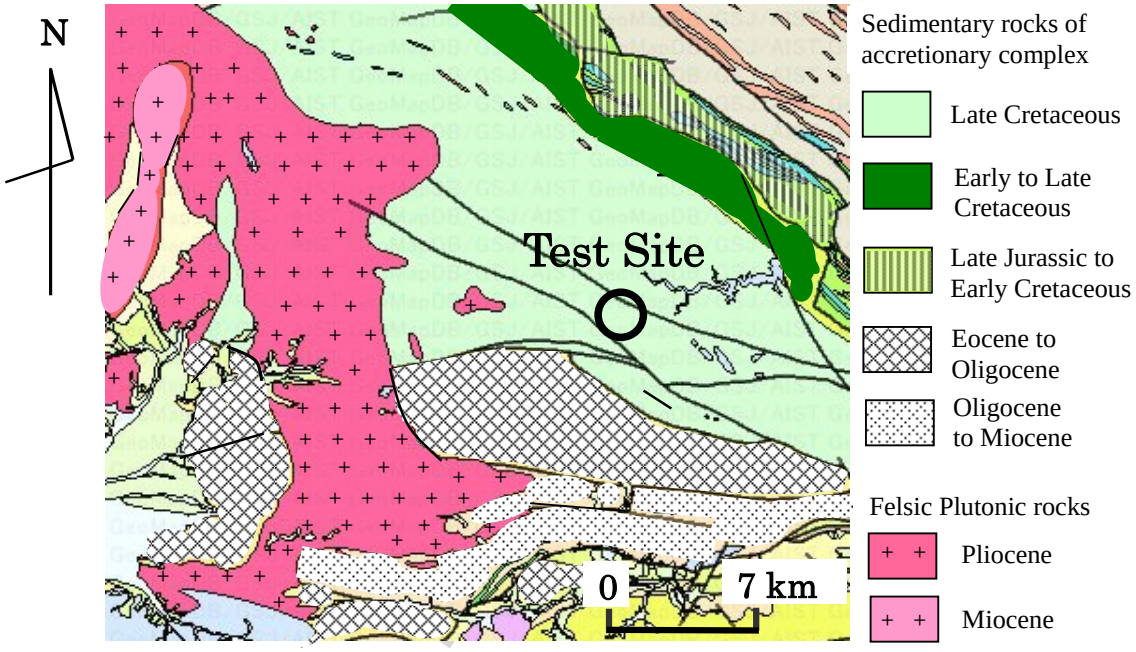

Figure 2 Geological map of a 35 × 35 km area around the test site. Source: Seamless Digital Geological Map of Japan, scale: 1:200,000 (modified). (Geological Survey of Japan, AIST, (ed.), 2007)

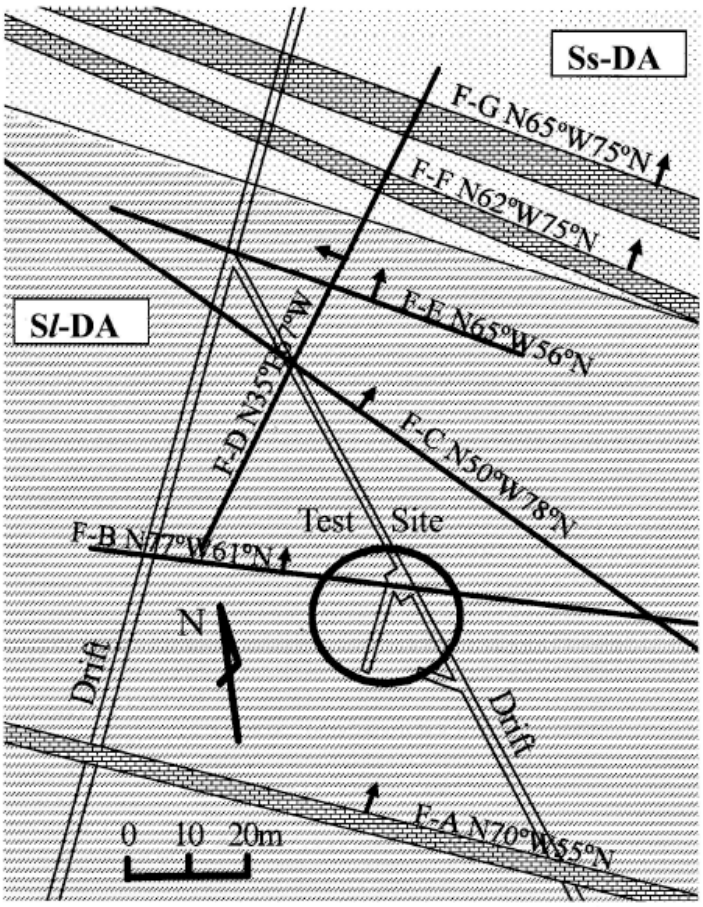

Figure 3 Geological map of a 100 × 100 m area around the test site. Solid circle indicates position of the test site. S*l*-DA: Slate-dominant alternation of slate and sandstone. Ss-DA: Sandstone-dominant alternation of slate and sandstone.

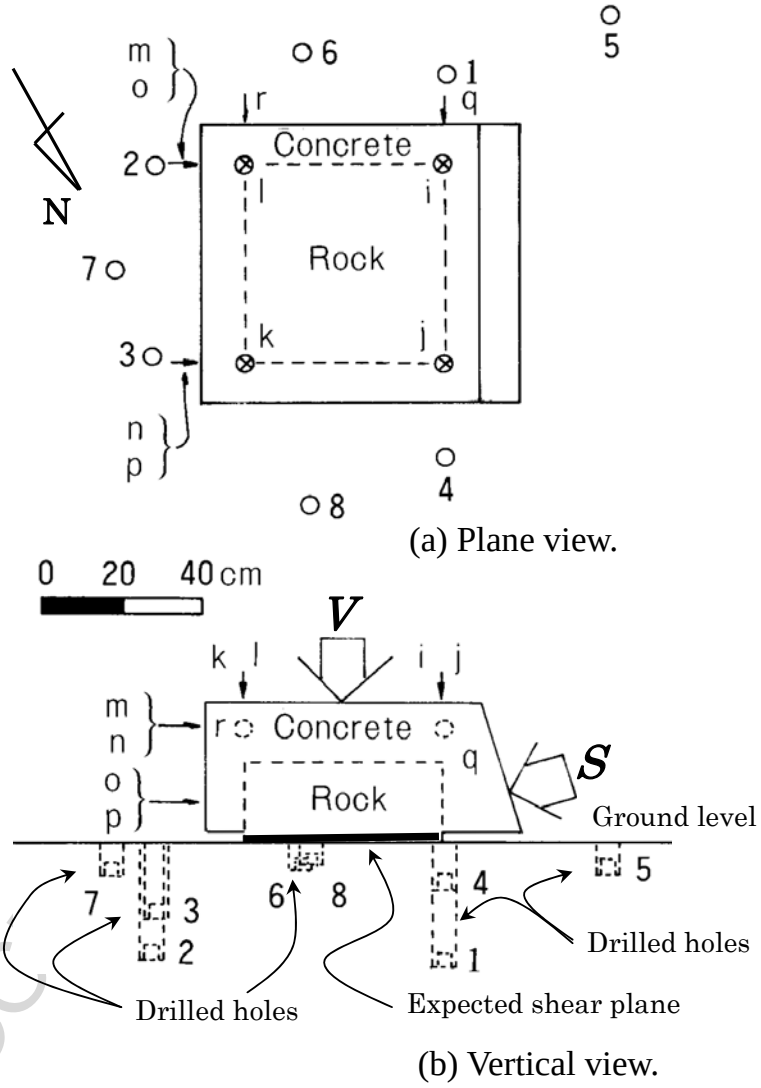

Figure 4 (a) Plane view and (b) vertical view of the test block for the in-situ direct shear test. Setting positions of the AE sensors (numbers 1 to 8) and displacement gauges (letters i to r) are also shown. Two large open arrows show the directions of vertical load, *V*, and shear load, *S*, which were applied to the test block.

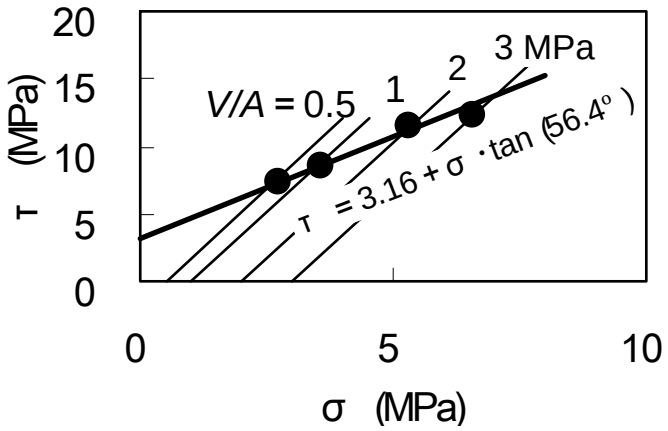

Figure 5 Results of the series of in-situ direct shear tests with the regression line showing a cohesion of 3.16 MPa and an internal friction angle of 56.4º. Four parallel thin solid lines indicate stress paths of respective tests, in which V is constant vertical load and A is area of the expected shear plane.

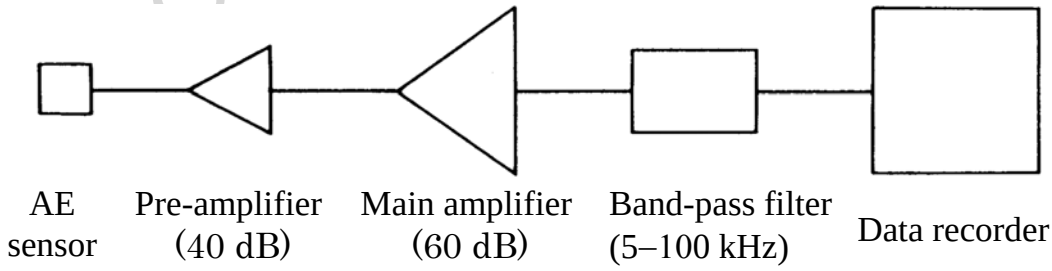

Figure 6 Schematic diagram of the AE measuring system.

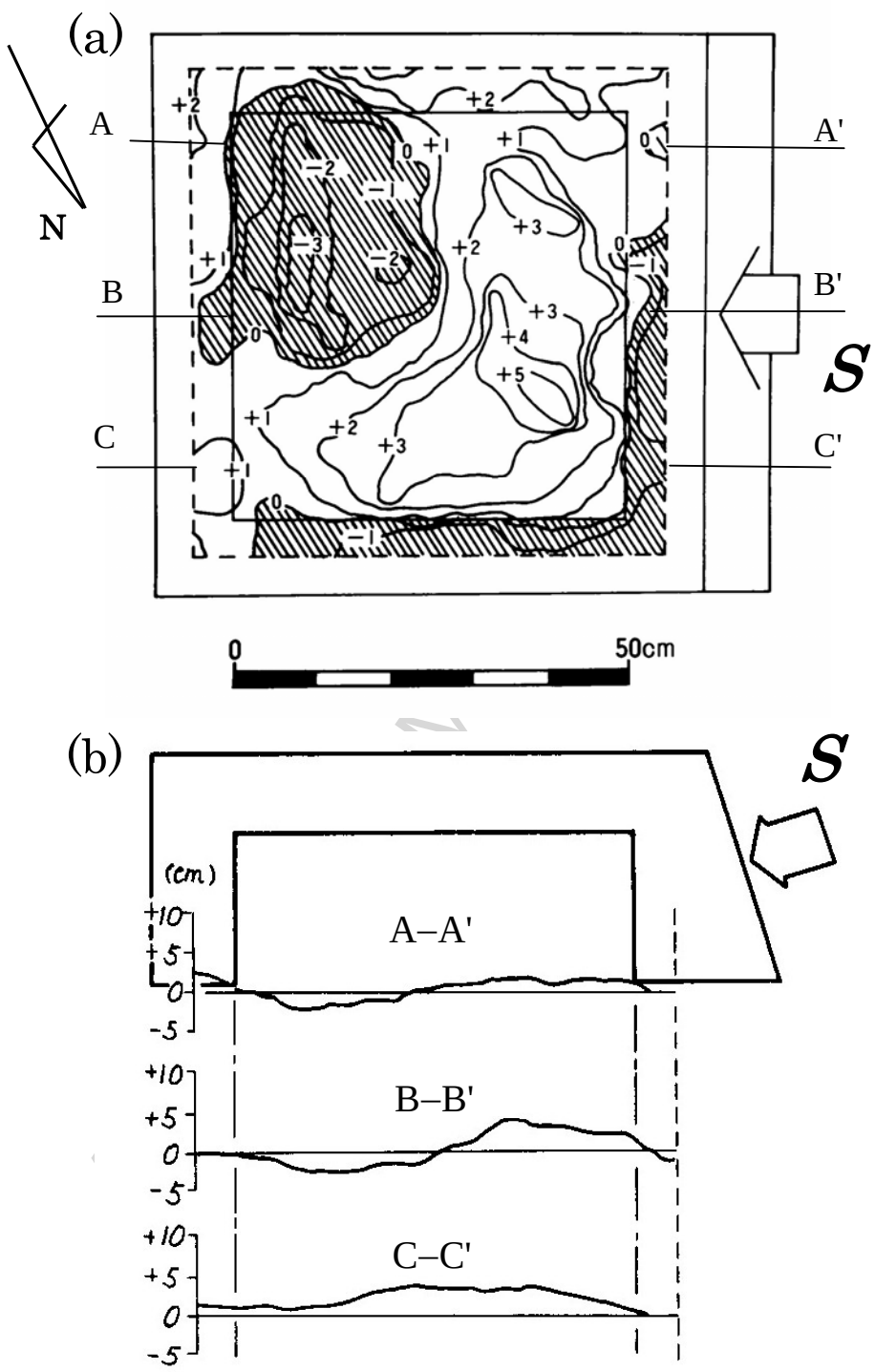

Figure 7 (a) Contour map of the fractured plane. Numerals indicate height in centimeters from the expected shear plane. Zero level is the ground surface around the specimen. Hatched area indicates concave regions lower than the expected shear plane. Large open arrow is the direction of the shear load. (b) Three sectional views along the lines A-A', B-B' and C-C' shown in (a).

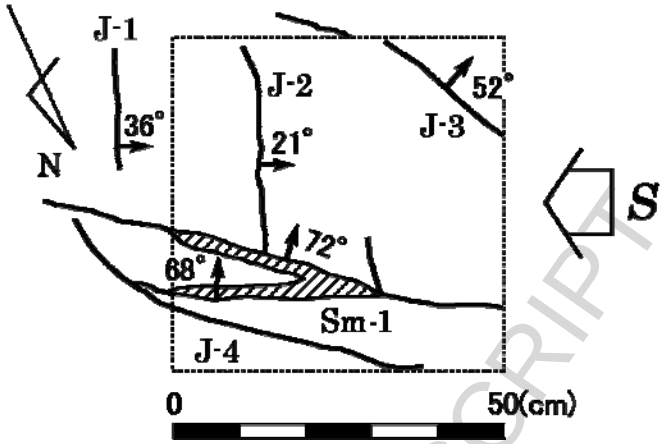

Figure 8 Sketch of the fractured surface plane. Solid lines indicate traces of joints J-1, J-2, J-3 and J-4 with arrows showing the directions of their dip angle. Hatched area indicates the loosening seam Sm-1.

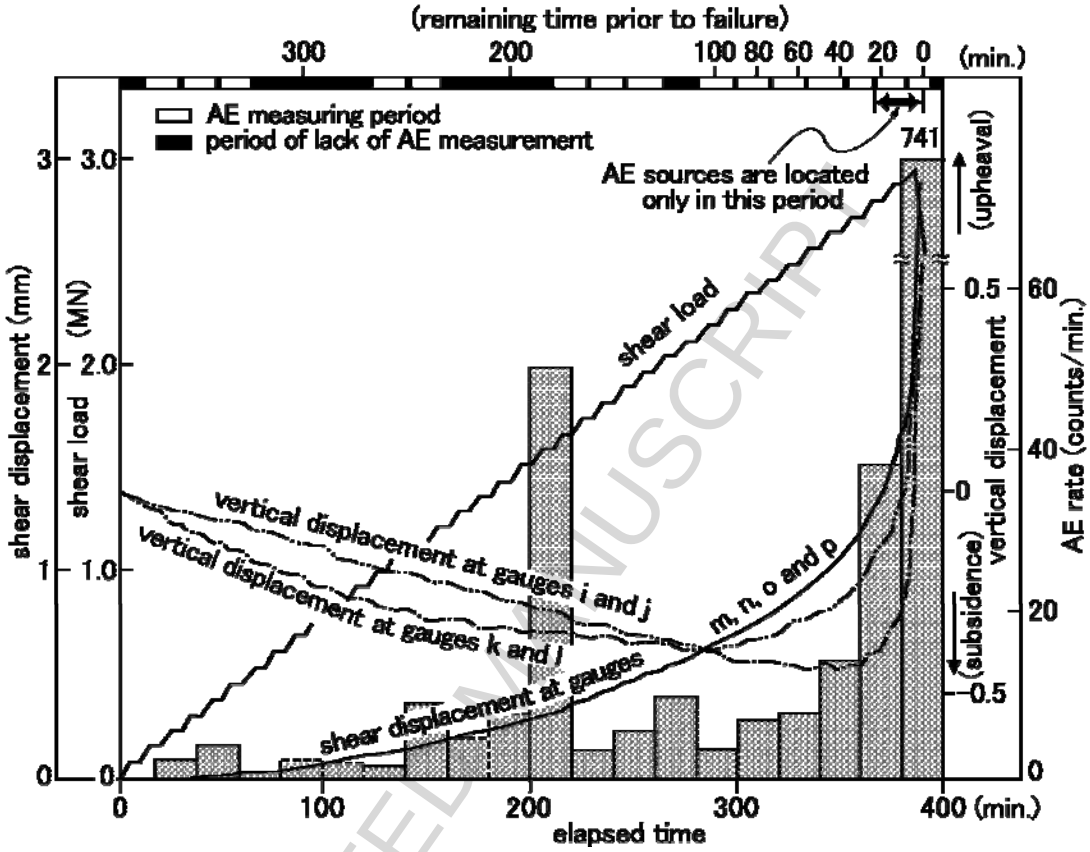

Figure 9 AE event rates, shear load, and shear and vertical displacements during the test run.

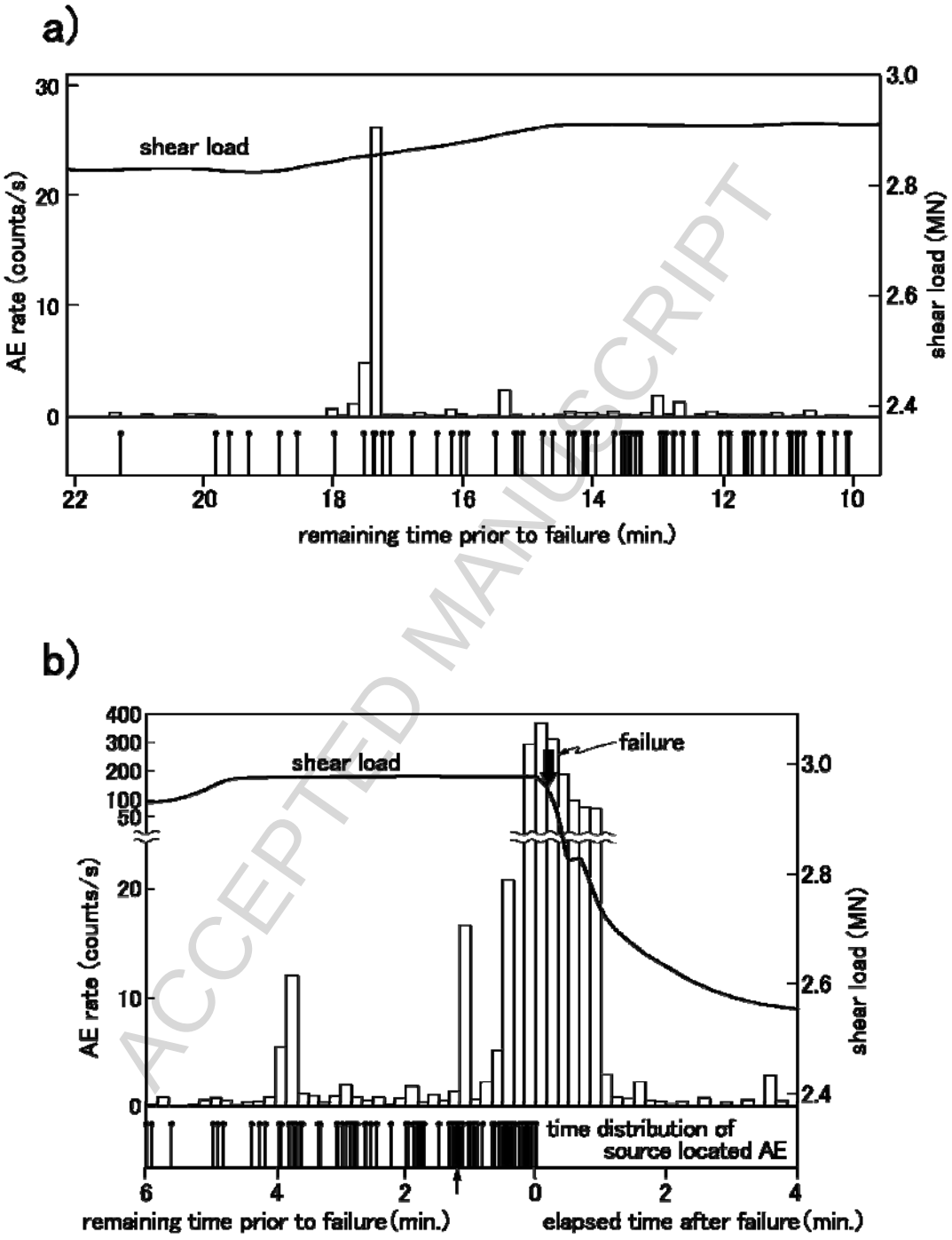

Figure 10 AE count rates and shear load for approximately 22 minutes prior to failure. Bars along the bottom lateral axes indicate occurrence of AE events for which epicenters are shown in Figure 12. (a) From 22 minutes 7 seconds to 9 minutes 37 seconds prior to the failure. (b) From 6 minutes prior to the failure to 4 minutes following the failure. Arrow at around 70 seconds prior to the failure indicates the occurrence time of the AE event for which waveforms are shown in Figure 11.

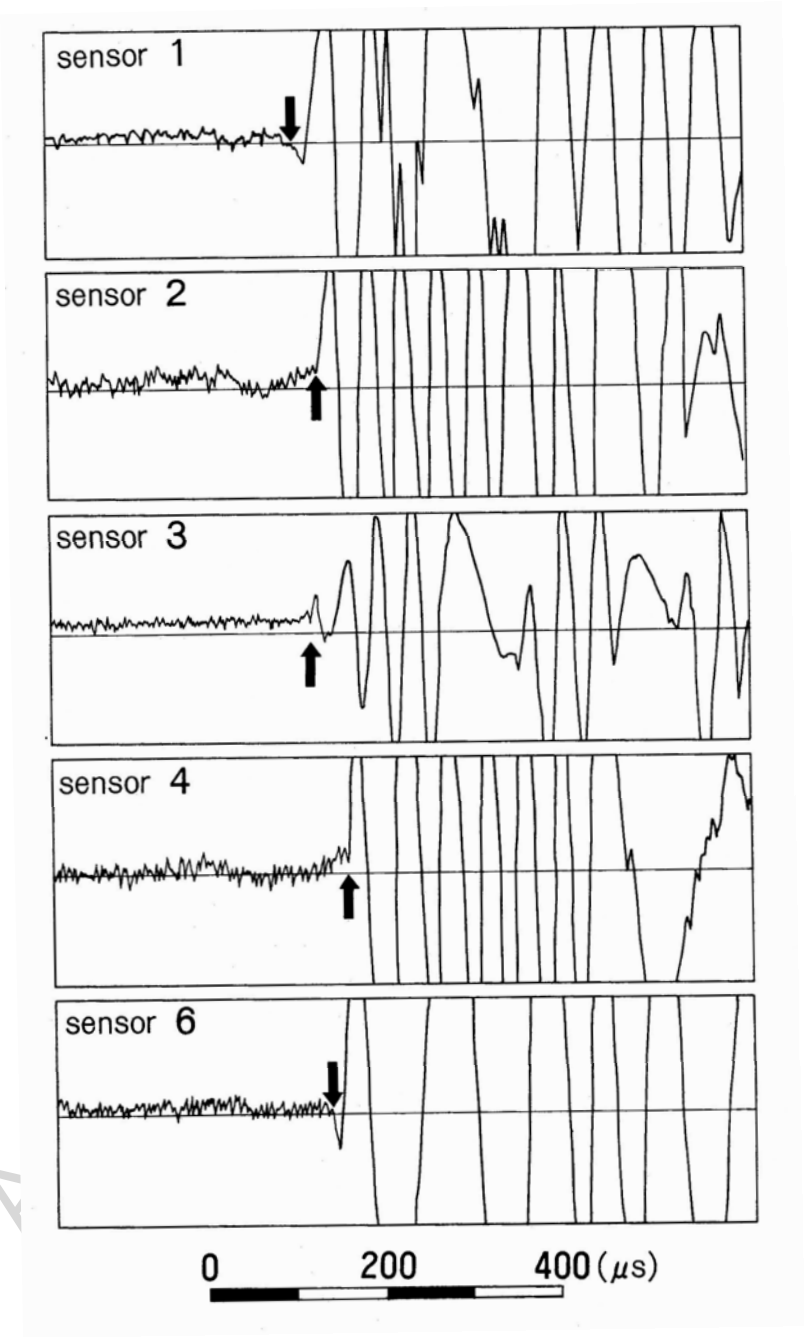

Figure 11 Example of recorded waveforms. Arrow on each waveform indicates arrival time that we interpret as the P-wave initial motion.

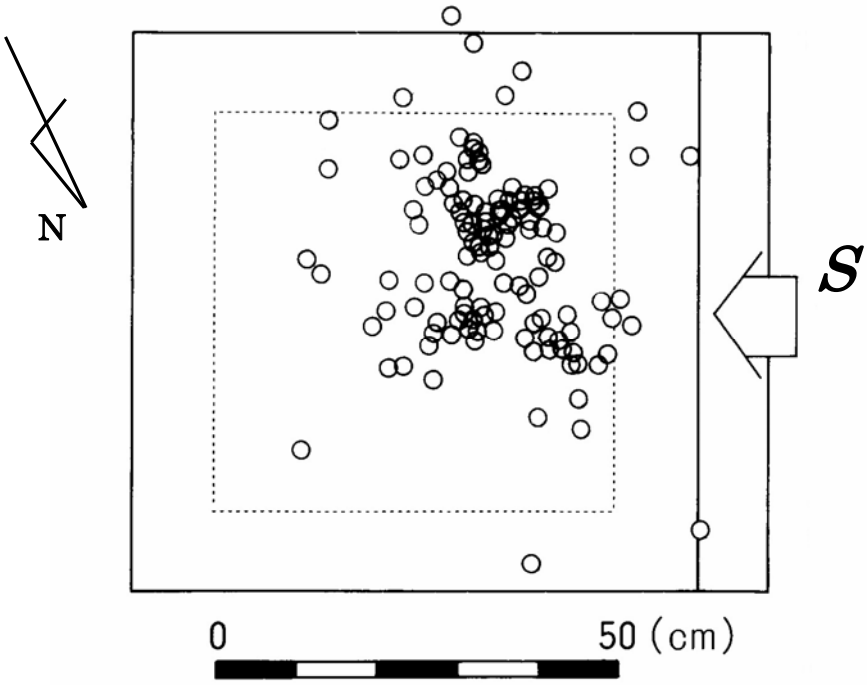

Figure 12 Distribution of all 154 AE epicenters located (open circles). Comparing this figure with Figure 8, the AE clustering region corresponds to the intact region bounded by the two joints J-2 and J-3, and the loosening seam Sm-1. Large open arrow indicates the direction of the applied shear load.

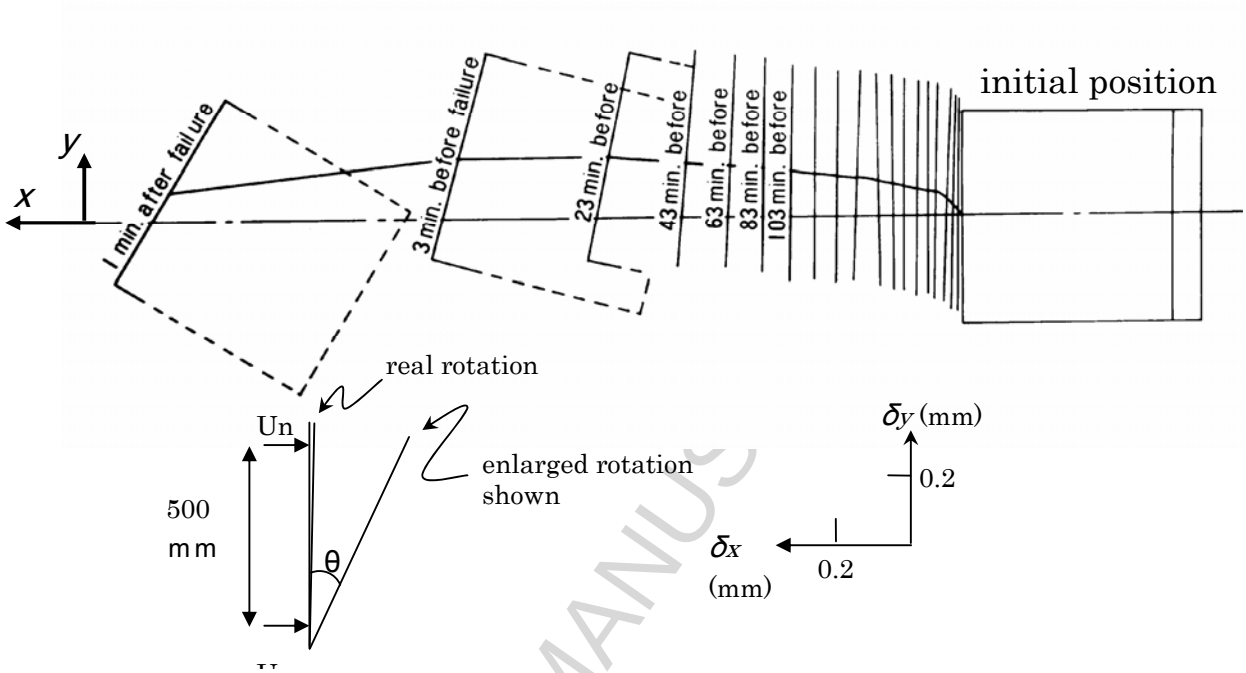

Figure 13 Plane view of the test block with time prior to the failure. Front of the test block is indicated by a solid line. Displacement is enlarged in comparison with the block size, as shown in the scale. The block rotation angle, θ, is also shown with an exaggeration of approximately 17.4 times larger than the real angle.

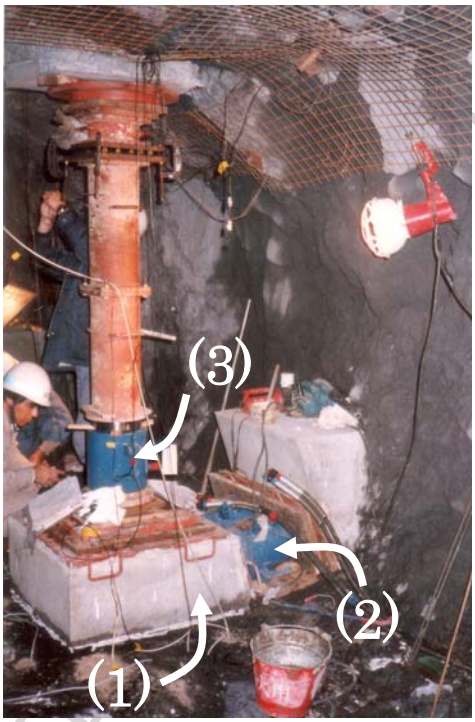

Photo 1 View of the direct shear test under preparation. (1) Test block. (2) Hydraulic ram for shear load *S*. (3) Hydraulic ram for vertical load *V*.

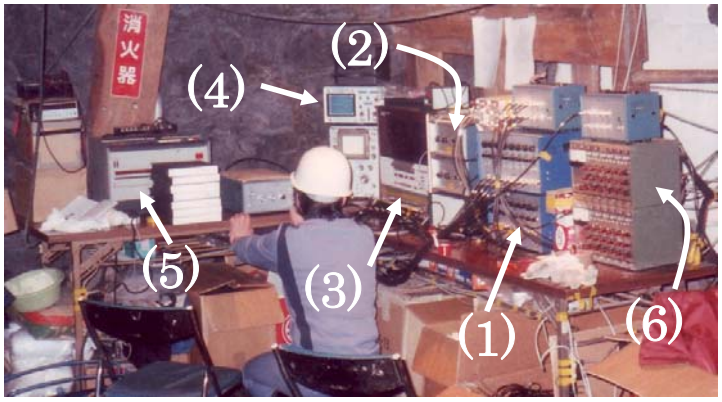

Photo 2 View of the AE-monitoring instruments. Since the test was conducted in 1984, the instruments are out of date. (1) Main amplifier. (2) Band-pass filter. (3) Data recorder. (4) Oscilloscope. (5) Oscillograph. (6) Amplifier for displacement gauges.

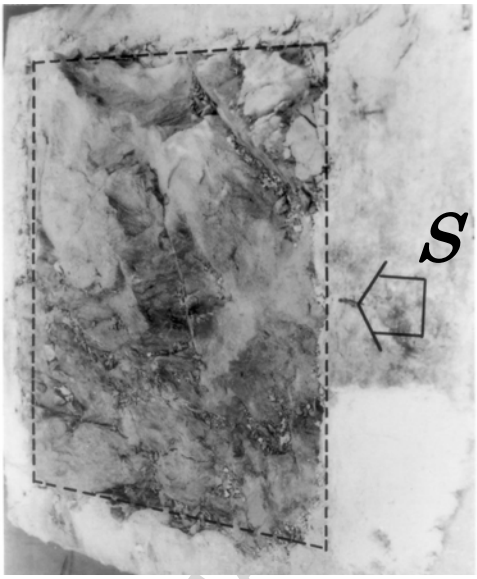

Photo 3 Fractured plane of the test block. This photo was printed by turning over the negative so that the right and the left hand sides along the direction of the shear load appear in the same position as in the other figures.